



INSTITUT DE FRANCE  
Académie des sciences

# *Comptes Rendus*

---

## *Mécanique*


Hoang Lan Ton-That, Hieu Nguyen-Van and Thanh Chau-Dinh

**Static and buckling analyses of stiffened plate/shell structures using the quadrilateral element SQ4C**

Volume 348, issue 4 (2020), p. 285-305.

<https://doi.org/10.5802/crmeca.7>

© Académie des sciences, Paris and the authors, 2020.  
*Some rights reserved.*

 This article is licensed under the  
CREATIVE COMMONS ATTRIBUTION 4.0 INTERNATIONAL LICENSE.  
<http://creativecommons.org/licenses/by/4.0/>



*Les Comptes Rendus. Mécanique sont membres du  
Centre Mersenne pour l'édition scientifique ouverte*  
[www.centre-mersenne.org](http://www.centre-mersenne.org)



---

# Static and buckling analyses of stiffened plate/shell structures using the quadrilateral element SQ4C

Hoang Lan Ton-That<sup>\*, a, b</sup>, Hieu Nguyen-Van<sup>b</sup> and Thanh Chau-Dinh<sup>a</sup>

<sup>a</sup> Department of Civil Engineering, Ho Chi Minh City University of Technology and Education, 01 Vo Van Ngan Street, Thu Duc District, Ho Chi Minh City, Viet Nam

<sup>b</sup> Department of Civil Engineering, Ho Chi Minh City University of Architecture, 196 Pasteur Street, District 3, Ho Chi Minh City, Viet Nam

*E-mails:* lan.tonthoang@uah.edu.vn, lantth.ncs@hcmute.edu.vn (H. L. Ton-That), hieu.nguyenvan@uah.edu.vn (H. Nguyen-Van), chdthanh@hcmute.edu.vn (T. Chau-Dinh)

**Abstract.** In the present study, a novel quadrilateral element, namely SQ4C, combined with the Timoshenko beam element is proposed for the static and buckling analyses of stiffened plate/shell structures. The idea behind these elements is a treatment for shear locking as well as membrane locking arising from the framework of the first-order shear deformation theory and a mesh with curved shell geometry. Formulations with eccentricity are also presented in this paper for the general case. The static and buckling analysis solutions and comparison with other available numerical solutions are presented to illustrate the robustness of the proposed elements to stiffened plate/shell structures. This paper also helps engineers in supplementing their knowledge.

**Keywords.** Static analysis, Buckling, Stiffened plate/shell, Strain smoothing technique, Shear locking, Membrane locking.

*Manuscript received 14th October 2019, revised 8th December 2019, accepted 6th January 2020.*

## 1. Introduction

Stiffened plate/shell structures with complex behaviours have been studied for many years [1–5]. At present, stiffened structures are commonly used in many fields of engineering such as civil, naval, aerospace, and so on. In [5] and [6], the orthotropic model and the grillage model were first introduced in stiffened plate problems, but they were not suitable. To overcome these restrictions, some authors modified them by not only separating the plate and stiffeners but also using some conditions at the contact surface between the plate and stiffeners. Based on these

---

\* Corresponding author.

points, analytical methods and numerical methods, such as the Ritz method [7–11], the mesh-free methods [12–14], the constraint method [15, 16], the finite difference method [17, 18], and the finite element methods [19–24], were used for solving stiffened structure problems. Some other developments that relate to stiffened plate/shell structures can be found in [25–29]. The inference that uses stiffeners to enhance stiffness is simple, but the practical stiffener design is difficult and complicated. An ineffective stiffener arrangement is unable not only to enhance the structure load capacity but also to reduce it. Thus it is very important to understand the mechanism by which a stiffener affects the structural behaviour as well as the stiffness. If stiffeners are used to increase the structural stiffness, it can be understood as the enhancement of buckling resistance and the reduction of structural deflection. Next, we mention the types of elements for plate/shell mesh as used in [30–49] with different strategies to analyse structures based on finite element procedures. In this study, a novel four-node quadrilateral element, namely SQ4C, is presented by using the strain smoothing technique and then combined with a strategy that reduces the effects of both shear locking and membrane locking. The static and buckling behaviours of stiffened plate/shell structures are the main focus of this paper. First, the theoretical formulations of this structure that relate to the effects of stiffener eccentricity or concentricity are established. Second, the element SQ4C based on the finite element formulation with many commendable properties such as (i) shear-locking-free, (ii) membrane-locking-free, and (iii) smooth strains related to cell smooth technology is presented. Third, the finite element formulations for the stiffener as well as for the total structure are investigated in Sections 4 and 5. Some numerical applications are presented in Section 6. Finally, some concluding remarks are given in Section 7.

## 2. Theoretical formulations

### 2.1. Formulation for plate

A plate with a stiffener is illustrated in Figure 1a. Let  $u_0$ ,  $v_0$ , and  $w_0$  be the displacements of a point located on the mid-surface. Let  $\beta_x$  and  $\beta_y$  be the in-plane rotations about the  $y$ -axis and the  $x$ -axis, respectively, and  $\beta_z$  be the drilling rotation around the  $z$ -axis. Based on the first-order shear deformation theory, the displacements  $u$ ,  $v$ , and  $w$  are defined by

$$u(x, y, z) = u_0(x, y) + z\beta_x(x, y), \quad (1)$$

$$v(x, y, z) = v_0(x, y) + z\beta_y(x, y), \quad (2)$$

$$w(x, y, z) = w_0(x, y). \quad (3)$$

The in-plane, bending, and shear strains of the plate are given by

$$\boldsymbol{\varepsilon}_{\text{inp}} = \begin{bmatrix} u_{0,x} \\ v_{0,y} \\ u_{0,y} + v_{0,x} \end{bmatrix} = \begin{bmatrix} \frac{\partial}{\partial x} & 0 & 0 & 0 & 0 & 0 \\ 0 & \frac{\partial}{\partial y} & 0 & 0 & 0 & 0 \\ \frac{\partial}{\partial y} & \frac{\partial}{\partial x} & 0 & 0 & 0 & 0 \end{bmatrix} \begin{bmatrix} u_0 \\ v_0 \\ w_0 \\ \beta_x \\ \beta_y \\ \beta_z \end{bmatrix} = \mathbf{O}_p^{\text{inp}} \mathbf{u}, \quad (4)$$

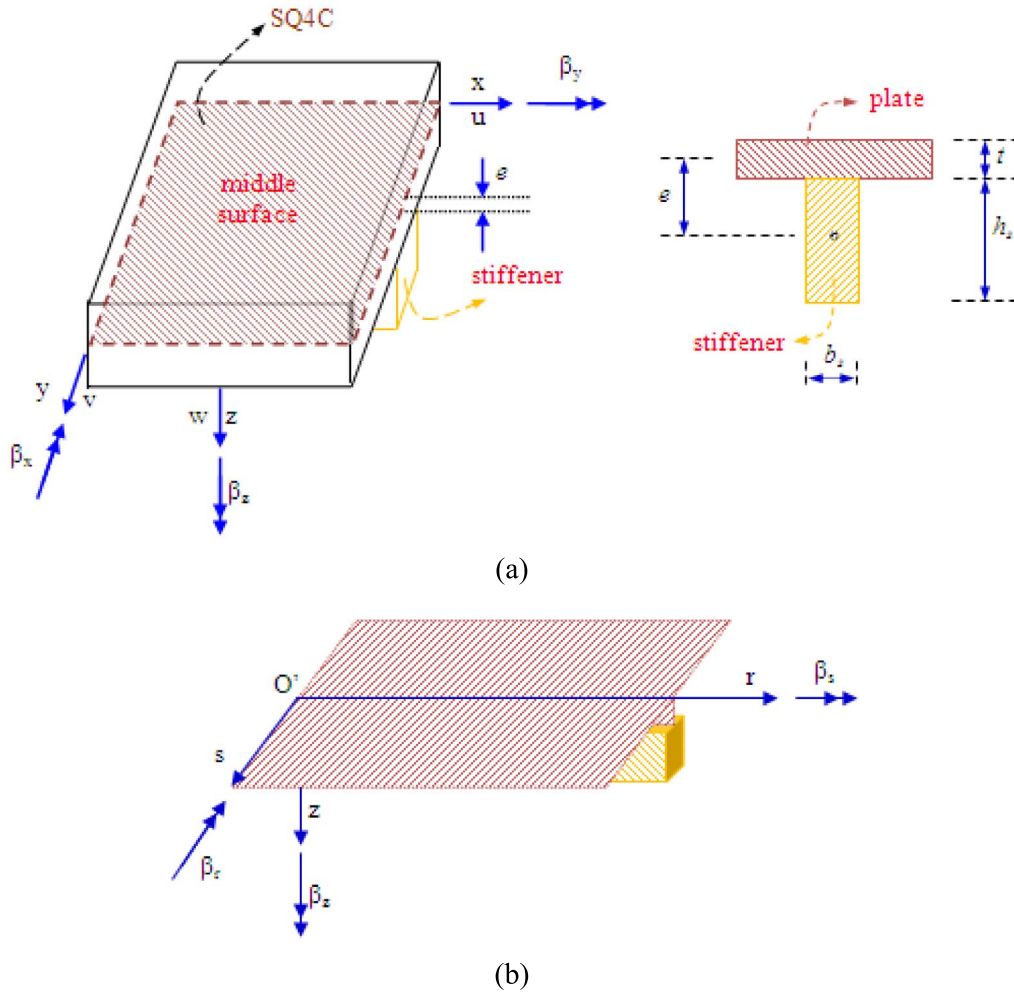


**Figure 1.** (a) The stiffened plate and (b) the stiffener with the local coordinate system.

$$\epsilon_b = \begin{bmatrix} \beta_{x,x} \\ \beta_{y,y} \\ \beta_{x,y} + \beta_{y,x} \end{bmatrix} = \begin{bmatrix} 0 & 0 & 0 & \frac{\partial}{\partial x} & 0 & 0 \\ 0 & 0 & 0 & 0 & \frac{\partial}{\partial y} & 0 \\ 0 & 0 & 0 & \frac{\partial}{\partial y} & \frac{\partial}{\partial x} & 0 \end{bmatrix} \begin{bmatrix} u_0 \\ v_0 \\ w_0 \\ \beta_x \\ \beta_y \\ \beta_z \end{bmatrix} = \mathbf{O}_p^b \mathbf{u}, \tag{5}$$

$$\epsilon_s = \begin{bmatrix} w_{,x} + \beta_x \\ w_{,y} + \beta_y \end{bmatrix} = \begin{bmatrix} 0 & 0 & \frac{\partial}{\partial x} & 1 & 0 & 0 \\ 0 & 0 & \frac{\partial}{\partial y} & 0 & 1 & 0 \end{bmatrix} \begin{bmatrix} u_0 \\ v_0 \\ w_0 \\ \beta_x \\ \beta_y \\ \beta_z \end{bmatrix} = \mathbf{O}_p^s \mathbf{u}, \tag{6}$$

where  $\mathbf{O}_p^{\text{inp}}$ ,  $\mathbf{O}_p^b$ , and  $\mathbf{O}_p^s$  are called the operational matrices and  $\mathbf{u} = [u_0 \ v_0 \ w_0 \ \beta_x \ \beta_y \ \beta_z]^T$  is the unknown vector of six independent field variables. With  $\epsilon_{\text{inp}}$ ,  $\epsilon_b$ , and  $\epsilon_s$  as mentioned above, the

energy of elastic strain is presented for the plate as follows:

$$\begin{aligned}
 U_{\text{plate}}^{\text{elas}} &= \frac{1}{2} \left( \iint_{\Omega} \boldsymbol{\varepsilon}_{\text{inp}}^T \mathbf{D}^{\text{inp}} \boldsymbol{\varepsilon}_{\text{inp}} \, d\Omega + \iint_{\Omega} \boldsymbol{\varepsilon}_b^T \mathbf{D}^{\text{ben}} \boldsymbol{\varepsilon}_b \, d\Omega + \iint_{\Omega} \boldsymbol{\varepsilon}_s^T \mathbf{D}^{\text{she}} \boldsymbol{\varepsilon}_s \, d\Omega \right) \\
 &= \frac{1}{2} \left( \iint_{\Omega} \mathbf{u}^T (\mathbf{O}_p^{\text{inp}})^T \mathbf{D}^{\text{inp}} \mathbf{O}_p^{\text{inp}} \mathbf{u} \, d\Omega + \iint_{\Omega} \mathbf{u}^T (\mathbf{O}_p^b)^T \mathbf{D}^{\text{ben}} \mathbf{O}_p^b \mathbf{u} \, d\Omega \right. \\
 &\quad \left. + \iint_{\Omega} \mathbf{u}^T (\mathbf{O}_p^s)^T \mathbf{D}^{\text{she}} \mathbf{O}_p^s \mathbf{u} \, d\Omega. \right) \tag{7}
 \end{aligned}$$

Here,

$$\mathbf{D}^{\text{inp}} = \frac{Et}{1-\nu^2} \begin{bmatrix} 1 & \nu & 0 \\ \nu & 1 & 0 \\ 0 & 0 & \frac{1-\nu}{2} \end{bmatrix}, \tag{8}$$

$$\mathbf{D}^{\text{ben}} = \frac{Et^3}{12(1-\nu^2)} \begin{bmatrix} 1 & \nu & 0 \\ \nu & 1 & 0 \\ 0 & 0 & \frac{1-\nu}{2} \end{bmatrix}, \tag{9}$$

$$\mathbf{D}^{\text{she}} = \frac{Et k}{2(1+\nu)} \begin{bmatrix} 1 & 0 \\ 0 & 1 \end{bmatrix} \tag{10}$$

are the material matrices with a correction factor  $k = 5/6$  and  $t$  is the thickness of the plate.

The energy of geometric strain that arises from in-plane pre-buckling stresses  $\bar{\boldsymbol{\sigma}}_0 = [\sigma_x^0 \ \sigma_y^0 \ \sigma_{xy}^0 \ 0 \ 0 \ 0]^T$  is calculated for the plate by

$$U_{\text{plate}}^{\text{geo}} = \iiint_V \bar{\boldsymbol{\sigma}}_0 \boldsymbol{\varepsilon}_p^{\text{geo}} \, dV, \tag{11}$$

where  $\boldsymbol{\varepsilon}_p^{\text{geo}}$  is called the geometric strain of the plate,

$$\boldsymbol{\varepsilon}_p^{\text{geo}} = \begin{bmatrix} \frac{1}{2}(w_{,x})^2 + \frac{z^2}{2}(\beta_{x,x})^2 + \frac{z^2}{2}(\beta_{y,x})^2 \\ \frac{1}{2}(w_{,y})^2 + \frac{z^2}{2}(\beta_{x,y})^2 + \frac{z^2}{2}(\beta_{y,y})^2 \\ (w_{,x})(w_{,y}) + z^2(\beta_{x,x})(\beta_{x,y}) + z^2(\beta_{y,x})(\beta_{y,y}) \\ 0 \\ 0 \\ 0 \end{bmatrix}. \tag{12}$$

By integrating through the thickness of the plate and noting that  $\Omega$  is a domain  $\subset R^2$  that depicts the middle surface  $Oxy$  of the plate,

$$U_{\text{plate}}^{\text{geo}} = \frac{1}{2} \iint_{\Omega} (\bar{\boldsymbol{\varepsilon}}_p^{\text{geo}})^T \bar{\boldsymbol{\sigma}}_0 (\bar{\boldsymbol{\varepsilon}}_p^{\text{geo}}) \, d\Omega. \tag{13}$$

This geometric strain of the plate can be rewritten as

$$U_{\text{plate}}^{\text{geo}} = \frac{1}{2} \iint_{\Omega} \mathbf{u}^T (\mathbf{O}_p^{\text{geo}})^T \bar{\boldsymbol{\sigma}}_0 \mathbf{O}_p^{\text{geo}} \mathbf{u} \, d\Omega \tag{14}$$

in which the matrices  $\widehat{\boldsymbol{\varepsilon}}_p^{\text{geo}}$  and  $\widehat{\boldsymbol{\sigma}}_0$  are given as

$$\widehat{\boldsymbol{\varepsilon}}_p^{\text{geo}} = \begin{bmatrix} 0 & 0 & \frac{\partial}{\partial x} & 0 & 0 & 0 \\ 0 & 0 & \frac{\partial}{\partial y} & 0 & 0 & 0 \\ 0 & 0 & 0 & \frac{\partial}{\partial x} & 0 & 0 \\ 0 & 0 & 0 & \frac{\partial}{\partial y} & 0 & 0 \\ 0 & 0 & 0 & 0 & \frac{\partial}{\partial x} & 0 \\ 0 & 0 & 0 & 0 & \frac{\partial}{\partial y} & 0 \end{bmatrix} \begin{bmatrix} u_o \\ v_o \\ w_o \\ \beta_x \\ \beta_y \\ \beta_z \end{bmatrix} = \mathbf{O}_p^{\text{geo}} \mathbf{u}, \tag{15}$$

$$\widehat{\boldsymbol{\sigma}}_0 = \begin{bmatrix} t\boldsymbol{\sigma}_0 & 0 & 0 \\ 0 & \frac{t^3}{12}\boldsymbol{\sigma}_0 & 0 \\ 0 & 0 & \frac{t^3}{12}\boldsymbol{\sigma}_0 \end{bmatrix} \tag{16}$$

with

$$\boldsymbol{\sigma}_0 = \begin{bmatrix} \sigma_x^0 & \sigma_{xy}^0 \\ \sigma_{xy}^0 & \sigma_y^0 \end{bmatrix}. \tag{17}$$

### 2.2. Formulation for stiffener

In Figure 1, the local coordinate  $O'rsz$  of the stiffener has an  $O'rs$  plane that coincides with the  $Oxy$  plane of the plate. At the contact surface, the displacements of the plate or shell structures are the same as the displacements of the stiffeners. By neglecting the lateral displacements and the rotations along the  $z$ -axis of the stiffener, the displacements of the stiffener in local coordinates are described by the middle surface displacements of the plate in the same coordinates. Then the elastic strain field of the stiffener is given by

$$\boldsymbol{\varepsilon}_{\text{stiff}}^{\text{elas}} = \begin{bmatrix} u_{r,r} + z\beta_{r,r} \\ u_{s,r} + z\beta_{s,r} \\ u_{z,r} + s\beta_{s,r} + \beta_r \end{bmatrix}. \tag{18}$$

The energy of elastic strain for the stiffener is presented as follows:

$$\begin{aligned} U_{\text{stiffener}}^{\text{elas}} &= \frac{1}{2} \int_l \iint_{A_{\text{stiff}}} (\boldsymbol{\varepsilon}_{\text{stiff}}^{\text{elas}})^T \mathbf{D}^{\text{stiff}} \boldsymbol{\varepsilon}_{\text{stiff}}^{\text{elas}} dA_{\text{stiff}} dl \\ &= \frac{1}{2} \int_l \left( GA_{\text{stiff}}(u_{z,r} + \beta_r)^2 + G(I_s + I_z)\beta_{s,r}^2 + EA_{\text{stiff}}(u_{r,r} + e\beta_{r,r})^2 \right) dl, \end{aligned} \tag{19}$$

where

$$\mathbf{D}^{\text{stiff}} = \begin{bmatrix} E & 0 & 0 \\ 0 & G & 0 \\ 0 & 0 & G \end{bmatrix} \tag{20}$$

and  $G$  and  $E$  are the elastic and shear moduli, respectively. Furthermore,  $I_s$  and  $I_z$  are the second moments of the stiffener cross-sectional area  $A_{\text{stiff}}$  related to the  $s$ -axis and the  $z$ -axis,

respectively, and  $e$  is the eccentricity between the middle surface of the plate and the neutral axis of the stiffener. The value  $GA_{\text{stiff}}(u_{s,r} + e\beta_{s,r})^2$  is neglected because the energies on the plane of the plate can be ignored. The energy of elastic strain of the stiffener is then rewritten in matrix form as

$$U_{\text{stiffener}}^{\text{elas}} = \frac{1}{2} \int_l (\widehat{\boldsymbol{\varepsilon}}_{\text{stiff}}^{\text{elas}})^T \widehat{\mathbf{D}}_{\text{stiff}} \widehat{\boldsymbol{\varepsilon}}_{\text{stiff}}^{\text{elas}} dl = \frac{1}{2} \int_l \mathbf{u}_{\text{stiff}}^T (\mathbf{O}_{\text{stiff}}^{\text{elas}})^T \widehat{\mathbf{D}}_{\text{stiff}} \mathbf{O}_{\text{stiff}}^{\text{elas}} \mathbf{u}_{\text{stiff}} dl \tag{21}$$

in which

$$\widehat{\mathbf{D}}_{\text{stiff}} = \begin{bmatrix} EA_{\text{stiff}} & 0 & 0 & 0 \\ 0 & EI_s & 0 & 0 \\ 0 & 0 & kGA_{\text{stiff}} & 0 \\ 0 & 0 & 0 & GI_{\text{venant}} \end{bmatrix}, \tag{22}$$

$$\widehat{\boldsymbol{\varepsilon}}_{\text{stiff}}^{\text{elas}} = \underbrace{\begin{bmatrix} \frac{\partial}{\partial r} & 0 & 0 & e \frac{\partial}{\partial r} & 0 & 0 \\ 0 & 0 & 0 & \frac{\partial}{\partial r} & 0 & 0 \\ 0 & 0 & \frac{\partial}{\partial r} & 1 & 0 & 0 \\ 0 & 0 & 0 & 0 & \frac{\partial}{\partial r} & 0 \end{bmatrix}}_{\widehat{\mathbf{O}}_{\text{stiff}}^{\text{elas}}} \underbrace{\begin{bmatrix} c_x & c_y & 0 & 0 & 0 & 0 \\ -c_y & c_x & 0 & 0 & 0 & 0 \\ 0 & 0 & 1 & 0 & 0 & 0 \\ 0 & 0 & 0 & c_x & c_y & 0 \\ 0 & 0 & 0 & -c_y & c_x & 0 \\ 0 & 0 & 0 & 0 & 0 & 0 \end{bmatrix}}_{\mathbf{Tr}} \mathbf{u}_{\text{stiff}}, \tag{23}$$

$$\mathbf{O}_{\text{stiff}}^{\text{elas}} = \widehat{\mathbf{O}}_{\text{stiff}}^{\text{elas}} \mathbf{Tr}. \tag{24}$$

Here,  $\mathbf{Tr}$  is called the transformation matrix and  $c_x$  and  $c_y$  are the direction cosines. Moreover,  $\mathbf{u}_{\text{stiff}} = [u_o^{\text{stiff}} \ v_o^{\text{stiff}} \ w_o^{\text{stiff}} \ \beta_x^{\text{stiff}} \ \beta_y^{\text{stiff}} \ \beta_z^{\text{stiff}}]^T$ , and St Venant’s torsion constant  $I_{\text{venant}}$  is used to replace the sum  $(I_s + I_z)$  for simplicity.

In the same manner, the energy of geometric strain that arises from in-plane pre-buckling stresses  $\widehat{\boldsymbol{\sigma}}_{0\text{stiff}} = [\sigma_x^0 \ 0 \ 0]^T$  is calculated for the stiffener as

$$U_{\text{stiffener}}^{\text{geo}} = \iiint_V \widehat{\boldsymbol{\sigma}}_{0\text{stiff}} \boldsymbol{\varepsilon}_{\text{stiff}}^{\text{geo}} dV, \tag{25}$$

where  $\boldsymbol{\varepsilon}_{\text{stiff}}^{\text{geo}}$  is called the geometric strain of the stiffener,

$$\boldsymbol{\varepsilon}_{\text{stiff}}^{\text{geo}} = \begin{bmatrix} \frac{1}{2}(u_{z,r})^2 + \frac{z^2}{2}(\beta_{r,r})^2 \\ 0 \\ 0 \end{bmatrix}. \tag{26}$$

By integrating through the cross-section of the stiffener, this energy of geometric strain can be computed as

$$U_{\text{stiffener}}^{\text{geo}} = \frac{1}{2} \int_l (\widehat{\boldsymbol{\varepsilon}}_{\text{stiff}}^{\text{geo}})^T \widehat{\boldsymbol{\sigma}}_{0\text{stiff}} \widehat{\boldsymbol{\varepsilon}}_{\text{stiff}}^{\text{geo}} dl = \frac{1}{2} \int_l \mathbf{u}_{\text{stiff}}^T (\mathbf{O}_{\text{stiff}}^{\text{geo}})^T \widehat{\boldsymbol{\sigma}}_{0\text{stiff}} \mathbf{O}_{\text{stiff}}^{\text{geo}} \mathbf{u}_{\text{stiff}} dl, \tag{27}$$

where the matrices  $\widehat{\boldsymbol{\varepsilon}}_{\text{stiff}}^{\text{geo}}$ ,  $\widehat{\boldsymbol{\sigma}}_{0\text{stiff}}$ , and  $\mathbf{O}_{\text{stiff}}^{\text{geo}}$  are given, respectively, by

$$\widehat{\boldsymbol{\varepsilon}}_{\text{stiff}}^{\text{geo}} = \underbrace{\begin{bmatrix} 0 & 0 & \frac{\partial}{\partial r} & 0 & 0 & 0 \\ 0 & 0 & 0 & \frac{\partial}{\partial r} & 0 & 0 \end{bmatrix}}_{\mathbf{O}_{\text{stiff}}^{\text{geo}}} \underbrace{\begin{bmatrix} c_x & c_y & 0 & 0 & 0 & 0 \\ -c_y & c_x & 0 & 0 & 0 & 0 \\ 0 & 0 & 1 & 0 & 0 & 0 \\ 0 & 0 & 0 & c_x & c_y & 0 \\ 0 & 0 & 0 & -c_y & c_x & 0 \\ 0 & 0 & 0 & 0 & 0 & 0 \end{bmatrix}}_{\mathbf{Tr}} \mathbf{u}_{\text{stiff}}, \tag{28}$$

$$\widehat{\boldsymbol{\sigma}}_{0\text{stiff}} = \begin{bmatrix} A_{\text{stiff}} \sigma_x^0 & 0 \\ 0 & (I_s + e^2 A_{\text{stiff}}) \sigma_x^0 \end{bmatrix}, \tag{29}$$

$$\mathbf{O}_{\text{stiff}}^{\text{geo}} = \mathbf{O}_{\text{stiff}}^{\text{geo}} \mathbf{Tr}. \tag{30}$$

### 3. Quadrilateral element SQ4C for plate

#### 3.1. In-plane part

The element with its mid-surface is separated into four domains, which are plotted in Figure 3. The assumed in-plane strain field is established by using the in-plane strains of these domains [44–46]. The centre point is denoted by “5” on the mid-surface of this element as shown in Figure 3a. The dependence of point “5” on four nodes “1”, “2”, “3”, and “4” is described as

$$\mathbf{x}_5 = \sum_{i=1}^4 \zeta_i \mathbf{x}_i, \tag{31}$$

where  $\zeta_i$  is calculated as

$$[\zeta_1 \ \zeta_2 \ \zeta_3 \ \zeta_4] = \frac{1}{2} \frac{A_{234}}{A_{234} + A_{124}} \begin{bmatrix} \frac{1}{3} & \frac{1}{3} & 0 & \frac{1}{3} \end{bmatrix} + \frac{1}{2} \frac{A_{124}}{A_{234} + A_{124}} \begin{bmatrix} 0 & \frac{1}{3} & \frac{1}{3} & \frac{1}{3} \end{bmatrix} + \frac{1}{2} \frac{A_{134}}{A_{134} + A_{123}} \begin{bmatrix} \frac{1}{3} & \frac{1}{3} & \frac{1}{3} & 0 \end{bmatrix} + \frac{1}{2} \frac{A_{123}}{A_{134} + A_{123}} \begin{bmatrix} \frac{1}{3} & 0 & \frac{1}{3} & \frac{1}{3} \end{bmatrix} \tag{32}$$

in which  $A_{234}$ ,  $A_{124}$ ,  $A_{134}$ , and  $A_{123}$  are called the areas of four domains “234”, “124”, “134”, and “123”, respectively.

By using the in-plane strains  $\tilde{\boldsymbol{\varepsilon}}_{ij}^{\text{inp(A)}}$ ,  $\tilde{\boldsymbol{\varepsilon}}_{ij}^{\text{inp(B)}}$ ,  $\tilde{\boldsymbol{\varepsilon}}_{ij}^{\text{inp(C)}}$ , and  $\tilde{\boldsymbol{\varepsilon}}_{ij}^{\text{inp(D)}}$  evaluated from four domains A, B, C, and D, four tying points are embedded into four positions as shown in Figures 2 and 3 to compute an assumed strain field, which alleviates membrane locking:

$$\tilde{\boldsymbol{\varepsilon}}_{ij}^{\text{inp(A)}} = \tilde{\mathbf{B}}_{\text{inp}}^{(\text{A})} \mathbf{q}_{\text{inp}}^{(\text{A})}, \quad \tilde{\boldsymbol{\varepsilon}}_{ij}^{\text{inp(B)}} = \tilde{\mathbf{B}}_{\text{inp}}^{(\text{B})} \mathbf{q}_{\text{inp}}^{(\text{B})}, \quad \tilde{\boldsymbol{\varepsilon}}_{ij}^{\text{inp(C)}} = \tilde{\mathbf{B}}_{\text{inp}}^{(\text{C})} \mathbf{q}_{\text{inp}}^{(\text{C})}, \quad \tilde{\boldsymbol{\varepsilon}}_{ij}^{\text{inp(D)}} = \tilde{\mathbf{B}}_{\text{inp}}^{(\text{D})} \mathbf{q}_{\text{inp}}^{(\text{D})} \tag{33}$$

and

$$\tilde{\boldsymbol{\varepsilon}}_{ij}^{\text{inp}} = \frac{1}{4} (\tilde{\boldsymbol{\varepsilon}}_{ij}^{\text{inp(A)}} + \tilde{\boldsymbol{\varepsilon}}_{ij}^{\text{inp(B)}} + \tilde{\boldsymbol{\varepsilon}}_{ij}^{\text{inp(C)}} + \tilde{\boldsymbol{\varepsilon}}_{ij}^{\text{inp(D)}}) + \frac{1}{2} (-\tilde{\boldsymbol{\varepsilon}}_{ij}^{\text{inp(D)}} + \tilde{\boldsymbol{\varepsilon}}_{ij}^{\text{inp(C)}}) \xi + \frac{1}{2} (-\tilde{\boldsymbol{\varepsilon}}_{ij}^{\text{inp(B)}} + \tilde{\boldsymbol{\varepsilon}}_{ij}^{\text{inp(A)}}) \eta. \tag{34}$$

The relationship between the in-plane strain field and the nodal displacement is then written as

$$\tilde{\boldsymbol{\varepsilon}}^{\text{inp}} = \tilde{\mathbf{B}}_{\text{inp}} \mathbf{q}_{\text{inp}}, \tag{35}$$



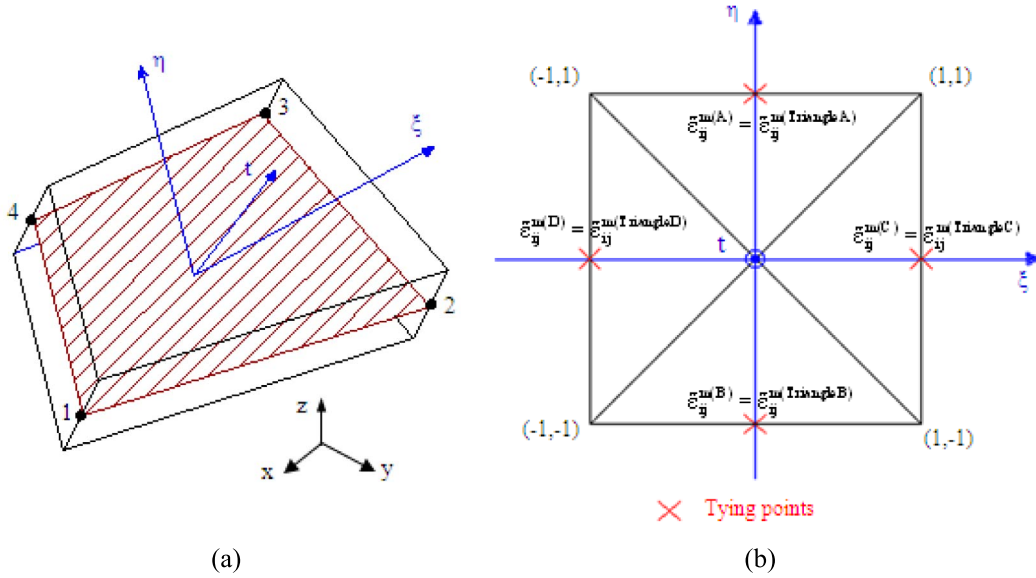


**Figure 2.** (a) A standard four-node quadrilateral element and (b) tying points on four sides.

where  $\tilde{\mathbf{B}}_{\text{inp}}$  is established by using four components  $\tilde{\mathbf{B}}_{\text{inp}}^{(A)}$ ,  $\tilde{\mathbf{B}}_{\text{inp}}^{(B)}$ ,  $\tilde{\mathbf{B}}_{\text{inp}}^{(C)}$ , and  $\tilde{\mathbf{B}}_{\text{inp}}^{(D)}$  of four triangular domains A, B, C, and D and  $\mathbf{q}_{\text{inp}}$  is also given by connected four components  $\mathbf{q}_{\text{inp}}^{(A)}$ ,  $\mathbf{q}_{\text{inp}}^{(B)}$ ,  $\mathbf{q}_{\text{inp}}^{(C)}$ , and  $\mathbf{q}_{\text{inp}}^{(D)}$  with the displacements at point “5” not being degrees of freedom in the element formulation:

$$\mathbf{q}_{\text{inp}(i)}^{(A)} = [u_{oi} \ v_{oi}], \quad i = 3, 4, 5, \tag{36}$$

$$\mathbf{q}_{\text{inp}(i)}^{(B)} = [u_{oi} \ v_{oi}], \quad i = 1, 2, 5, \tag{37}$$

$$\mathbf{q}_{\text{inp}(i)}^{(C)} = [u_{oi} \ v_{oi}], \quad i = 2, 3, 5, \tag{38}$$

$$\mathbf{q}_{\text{inp}(i)}^{(D)} = [u_{oi} \ v_{oi}], \quad i = 1, 4, 5. \tag{39}$$

Note that the in-plane displacement vector of the point “5” is absolutely approximated from the nodal displacements as

$$\mathbf{q}_{\text{inp}5} = \sum_{i=1}^4 c_i \mathbf{q}_{\text{inp}(i)}, \tag{40}$$

$$\mathbf{q}_{\text{inp}(i)} = [u_{oi} \ v_{oi}]. \tag{41}$$

### 3.2. Bending part

The bending strain is computed by using the cell-based smoothed method [35,37] and as shown in Figure 4. The quadrilateral element domain is further divided into *n<sub>ce</sub>* smoothing cells. The bending strain field is smoothed by a weighted average of the original bending strain using the strain smoothing operation for each smoothing cell and applying the divergence theorem:

$$\tilde{\boldsymbol{\varepsilon}}^b(x_C) = \int_{\Omega_C} \boldsymbol{\varepsilon}^b(x) \Phi(x - x_C) \, d\Omega = \frac{1}{2A_C} \int_{\Gamma_C} (\beta_i n_j + \beta_j n_i) \, d\Gamma, \tag{42}$$

where  $x_C$  is an arbitrary point,  $\Omega_C$  is the smoothing cell domain,  $\beta_i$  is the in-plane rotation,  $n_i$  is the component of the outward unit vector normal to the boundary  $\Gamma_C$  of the smoothing domain  $\Omega_C$ , and  $\Phi$  is a smoothing function that satisfies at least the unity property  $\int_{\Omega_C} \Phi \, d\Omega = 1$  as well

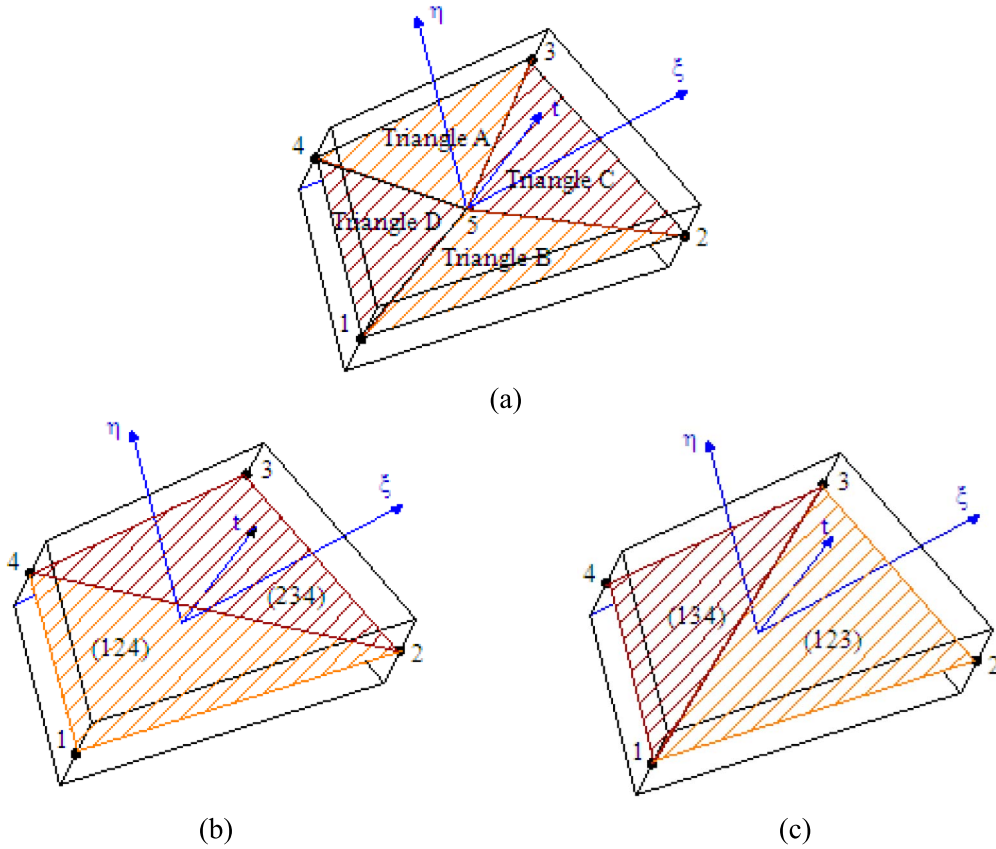


**Figure 3.** (a) Four domains on the mid-surface and (b) four other domains to determine point “5”.

as  $\Phi(x - x_C) = 1/A_C$  with  $x \in \Omega_C$  and  $\Phi(x - x_C) = 0$  with  $x \notin \Omega_C$ . The area of the smoothing cell is clearly calculated as  $A_C = \int_{\Omega_C} d\Omega$ .

The relationship between the smoothed bending strain field and the nodal displacement is then written as

$$\tilde{\varepsilon}^b = \tilde{\mathbf{B}}_b \mathbf{q}_b, \tag{43}$$

where

$$\tilde{\mathbf{B}}_{bi} = \frac{1}{A_C} \int_{\Gamma_C} \begin{pmatrix} 0 & N_i n_x & 0 \\ 0 & 0 & N_i n_y \\ 0 & N_i n_y & N_i n_x \end{pmatrix} d\Gamma, \tag{44}$$

$$\mathbf{q}_{bi} = [w_{0i} \ \beta_{xi} \ \beta_{yi}]. \tag{45}$$

Here,  $n_x$  and  $n_y$  are the components of the vector normal to the boundary  $\Gamma_C$ .

### 3.3. Shear part

Based on the attenuation of the shear-locking phenomenon under an assumption of constant transverse shear strains along four sides [41–43] and as shown in Figure 5, the transverse shear

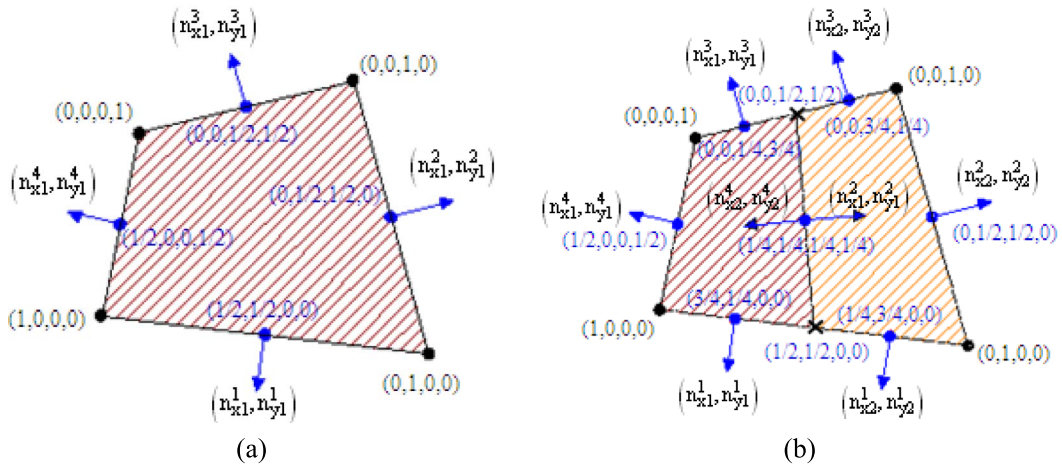


**Figure 4.** Subdivision of elements into *nce* smoothing cells and the values of shape functions at nodes in the format  $(N_1, N_2, N_3, N_4)$ .

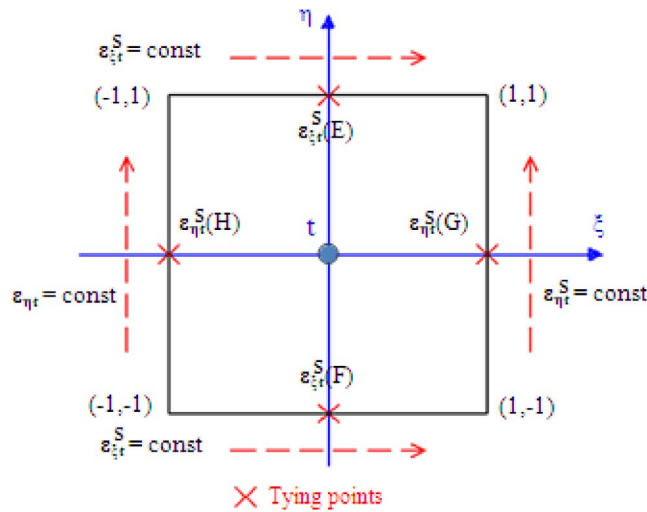


**Figure 5.** Four tying points (E), (F), (G), and (H).

strain field is given as

$$\begin{aligned} \tilde{\epsilon}_{\xi t}^s &= \frac{1}{2}(1 + \eta)\epsilon_{\xi t}^{s(E)} + \frac{1}{2}(1 - \eta)\epsilon_{\xi t}^{s(F)}, \\ \tilde{\epsilon}_{\eta t}^s &= \frac{1}{2}(1 + \xi)\epsilon_{\eta t}^{s(G)} + \frac{1}{2}(1 - \xi)\epsilon_{\eta t}^{s(H)}. \end{aligned} \tag{46}$$

Here,  $\epsilon_{\xi t}^{s(E)}$ ,  $\epsilon_{\xi t}^{s(F)}$ ,  $\epsilon_{\xi t}^{s(G)}$ , and  $\epsilon_{\xi t}^{s(H)}$  are four transverse shear strains directly computed from the displacement approximation at points (E), (F), (G), and (H), respectively.

The shear matrix can be presented as

$$\tilde{\mathbf{B}}_{si} = \begin{bmatrix} x_{,\xi} & y_{,\xi} \\ x_{,\eta} & y_{,\eta} \end{bmatrix}^{-1} \begin{bmatrix} N_{i,\xi} & b_i^{11} N_{i,\xi} & b_i^{12} N_{i,\xi} \\ N_{i,\eta} & b_i^{21} N_{i,\eta} & b_i^{22} N_{i,\eta} \end{bmatrix}, \tag{47}$$

where  $b_i^{11} = \xi_i x_{,\xi}^{R_1}$ ,  $b_i^{12} = \xi_i y_{,\xi}^{R_1}$ ,  $b_i^{21} = \eta_i x_{,\eta}^{R_2}$ , and  $b_i^{22} = \eta_i y_{,\eta}^{R_2}$  in which  $\xi_i \in \{-1 \ 1 \ 1 \ -1\}$ ,  $\eta_i \in \{-1 \ -1 \ 1 \ 1\}$ , and  $(i, R_1, R_2) \in \{(1, F, H), (2, F, G), (3, E, G), (4, E, H)\}$ .

### 3.4. Combination of three parts

Due to the appearance of the drilling rotation  $\beta_z$ , we used the Allman strategy that is detailed in the original reference [50] or our other paper [37] for independent interpolation. The in-plane stiffness matrix that is achieved in Section 3.1 is added by the new component  $\gamma \int_{\Omega} \mathbf{b}^T \mathbf{b} \, d\Omega$ . The positive penalty parameter  $\gamma = G$  is chosen in this study as follows [50]:

$$\mathbf{b}_i = \begin{bmatrix} -\frac{1}{2} N_{i,y} \\ -\frac{1}{2} N_{i,x} \\ -\frac{1}{2} (N x_{i,y} + N y_{i,x}) - N_i \end{bmatrix}, \tag{48}$$

$$N_i(\xi, \eta) = \frac{1}{4} (1 + \xi_i \xi) (1 + \eta_i \eta), \quad i = 1, 2, 3, 4, \tag{49}$$

$$N x_i = \frac{1}{8} (y_{ij} N_l - y_{ik} N_m) \quad \text{and} \quad N y_i = \frac{1}{8} (x_{ij} N_l - x_{ik} N_m), \tag{50}$$

$$x_{ij} = x_j - x_i \quad \text{and} \quad y_{ij} = y_j - y_i, \tag{51}$$

$$\text{Matlab code definition: } i = 1, 2, 3, 4; \quad m = i + 4; \tag{52}$$

$$l = m - 1 + 4 \text{ floor}(1/i); \quad k = \text{mod}(m, 4) + 1; \quad j = l - 4.$$

Finally, the global stiffness matrix  $\tilde{\mathbf{K}}_{\text{plate}}$  is obtained as

$$\tilde{\mathbf{K}}_{\text{plate}} = \tilde{\mathbf{K}}_{\text{inp}} + \tilde{\mathbf{K}}_b + \tilde{\mathbf{K}}_s, \tag{53}$$

where

$$\tilde{\mathbf{K}}_{\text{inp}} = \int_{\Omega} \tilde{\mathbf{B}}_{\text{inp}}^T \mathbf{D}^{\text{inp}} \tilde{\mathbf{B}}_{\text{inp}} \, d\Omega + \gamma \int_{\Omega} \mathbf{b}^T \mathbf{b} \, d\Omega, \tag{54}$$

$$\tilde{\mathbf{K}}_b = \int_{\Omega} \tilde{\mathbf{B}}_b^T \mathbf{D}^b \tilde{\mathbf{B}}_b \, d\Omega = \sum_i^{nce} \tilde{\mathbf{B}}_{bi}^T \mathbf{D}^b \tilde{\mathbf{B}}_{bi} \mathbf{A}_C, \tag{55}$$

$$\tilde{\mathbf{K}}_s = \int_{\Omega} \tilde{\mathbf{B}}_s^T \mathbf{D}^s \tilde{\mathbf{B}}_s \, d\Omega. \tag{56}$$

Here, *nce* is the number of smoothing cells; note that *nce* = 2 in order to obtain a suitable rank. For buckling analysis, the smoothed geometric stiffness matrix of the plate can be obtained as

$$\tilde{\mathbf{K}}_{\text{geo-plate}} = \int_{\Omega} \tilde{\mathbf{B}}_{\text{geo}}^T \bar{\boldsymbol{\sigma}}_0 \tilde{\mathbf{B}}_{\text{geo}} \, d\Omega = \sum_i^{nce} \tilde{\mathbf{B}}_{\text{geoi}}^T \bar{\boldsymbol{\sigma}}_0 \tilde{\mathbf{B}}_{\text{geoi}} \mathbf{A}_C, \tag{57}$$

where

$$\tilde{\mathbf{B}}_{\text{geoi}} = \frac{1}{A_C} \int_{\Gamma_C} \begin{bmatrix} N_i n_x & 0 & 0 \\ N_i n_y & 0 & 0 \\ 0 & N_i n_x & 0 \\ 0 & N_i n_y & 0 \\ 0 & 0 & N_i n_x \\ 0 & 0 & N_i n_y \end{bmatrix} d\Gamma. \tag{58}$$

Note that *nce* = 1 in this case.

## 4. Timoshenko beam element for stiffener

By using the two-node isoparametric Timoshenko beam element to model the stiffener, the vector of displacement field on the *e*th element is presented as

$$\mathbf{u}_{\text{stiff}}^{el} = \sum_{k=1}^2 \Psi_k \mathbf{I}_6 \mathbf{q}_{\text{stiff}}^k, \tag{59}$$

where  $\mathbf{q}_{\text{stiff}}^k = [u_r \ u_s \ u_z \ \beta_r \ \beta_s \ \beta_z]^T$  is the displacement vector of the  $k$ th node of the  $el$ th element and  $\Psi_k$  with  $k = 1, 2$  are the linear shape functions in natural coordinates defined as

$$\Psi_1 = \frac{1}{2}(1 - \xi), \quad \Psi_2 = \frac{1}{2}(1 + \xi), \quad \xi \in [-1, 1]. \tag{60}$$

We divide the stiffener into  $n_{\text{stiff}}$  elements. Then the stiffness and geometric matrices are given as

$$\tilde{\mathbf{K}}_{\text{stiff}} = \sum_{el=1}^{n_{\text{stiff}}} \tilde{\mathbf{K}}_{\text{stiff}}^{el}, \tag{61}$$

$$\tilde{\mathbf{K}}_{\text{geo-stiff}} = \sum_{el=1}^{n_{\text{stiff}}} \tilde{\mathbf{K}}_{\text{geo-stiff}}^{el}, \tag{62}$$

where

$$\tilde{\mathbf{K}}_{\text{stiff}}^{el} = \int_l (\mathbf{O}_{\text{stiff}}^{\text{elas}} \boldsymbol{\Psi})^T \widehat{\mathbf{D}}_{\text{stiff}} \mathbf{O}_{\text{stiff}}^{\text{elas}} \boldsymbol{\Psi} dl, \tag{63}$$

$$\tilde{\mathbf{K}}_{\text{geo-stiff}}^{el} = \int_l (\mathbf{O}_{\text{stiff}}^{\text{geo}} \boldsymbol{\Psi})^T \widehat{\boldsymbol{\sigma}}_{0\text{stiff}} \mathbf{O}_{\text{stiff}}^{\text{geo}} \boldsymbol{\Psi} dl. \tag{64}$$

### 5. Finite element formulations for static and buckling analyses

Based on the above sections, the stiffness and geometric matrices of the stiffened structures are calculated:

$$\tilde{\mathbf{K}}_{\text{struc}} = \tilde{\mathbf{K}}_{\text{plate}} + \mathbf{T}^T \tilde{\mathbf{K}}_{\text{stiff}} \mathbf{T}, \tag{65}$$

$$\tilde{\mathbf{K}}_{\text{geo-struc}} = \tilde{\mathbf{K}}_{\text{geo-plate}} + \mathbf{T}^T \tilde{\mathbf{K}}_{\text{geo-stiff}} \mathbf{T}, \tag{66}$$

where  $\mathbf{T}$  is the transformation matrix as given by [12, 13, 22]. For the general case, we can establish a stiffener that is placed askew an angle to the  $x$ -axis by modifying this transformation matrix.

For static analysis, we use the formulation

$$\tilde{\mathbf{K}}_{\text{struc}} \mathbf{q} = \mathbf{F}. \tag{67}$$

In addition, for buckling analysis, the formulation is presented as

$$(\tilde{\mathbf{K}}_{\text{struc}} - \lambda_{\text{cr}} \tilde{\mathbf{K}}_{\text{geo-struc}}) \mathbf{q} = 0. \tag{68}$$

### 6. Numerical examples

Six numerical examples are presented in this section to show the efficiency and effectiveness of the proposed elements. Obviously, these solutions of static and buckling analyses are compared with other available results. The simply supported boundary conditions are expressed as  $u_0 = w_0 = \beta_x = \beta_z = 0$  on edges in the  $x$ -direction and  $v_0 = w_0 = \beta_y = \beta_z = 0$  on edges in the  $y$ -direction for plate examples. Furthermore, the rigid diaphragm boundary conditions are expressed as  $u_0 = v_0 = w_0 = \beta_y = \beta_z = 0$  on curved edges along the  $y$ -direction for the shell roof.

#### 6.1. Static analysis

First, we consider a simply supported stiffened plate structure that is plotted in Figure 6. A uniform load  $q = 6.89476 \times 10^{-3}$  N/mm<sup>2</sup> is applied on the top surface of this structure. The material properties  $E = 1.1721 \times 10^5$  N/mm<sup>2</sup> and  $\nu = 0.3$  are assumed to be the same in the plate and the stiffener. The plate is discretized using  $4 \times 4, 6 \times 6, 8 \times 8, 10 \times 10, 12 \times 12,$  and  $14 \times 14$  meshes for this study. The normalized central deflections  $\bar{w} = w_{0\text{central}} / (qL^4 / 100D)$  of this structure based on these SQ4C elements for the case of the eccentric plate are presented in Table 1. It

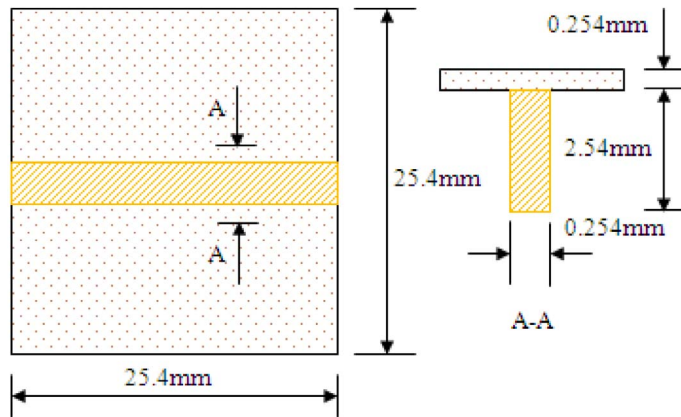


**Figure 6.** The square plate stiffened by one stiffener.

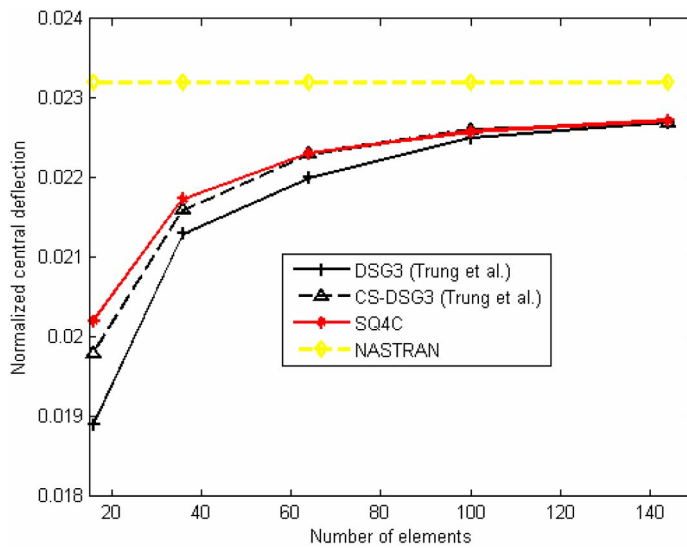


**Figure 7.** The convergence of the normalized central deflection.

**Table 1.** Comparison of the normalized deflection at the central point

| Mesh    | Central deflection       |             |              |         |
|---------|--------------------------|-------------|--------------|---------|
|         | Trung <i>et al.</i> [22] | Rossow [15] | NASTRAN [22] | SQ4C    |
| 4 × 4   | 0.0198                   | -           | -            | 0.02016 |
| 6 × 6   | 0.0216                   | -           | -            | 0.02171 |
| 8 × 8   | 0.0223                   | 0.0213      | 0.0232       | 0.02230 |
| 10 × 10 | 0.0226                   | -           | -            | 0.02257 |
| 12 × 12 | 0.0227                   | -           | -            | 0.02272 |
| 14 × 14 | -                        | -           | -            | 0.02281 |

can be seen that these solutions are in good agreement with the solutions of Rossow [15], Trung *et al.* [22], and the NASTRAN software [22] as shown in Table 1 and Figure 7.

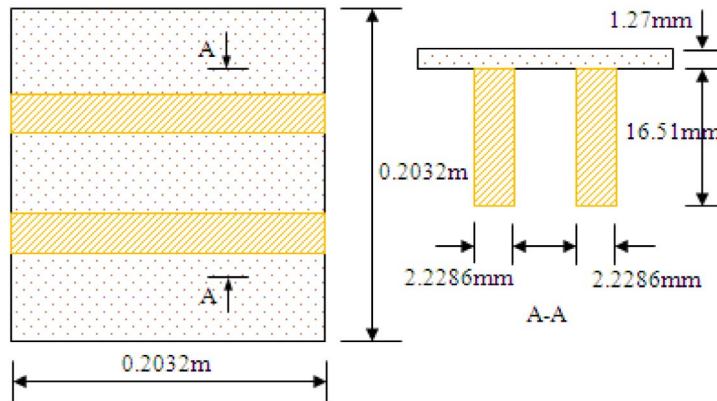


**Figure 8.** The square plate stiffened by two stiffeners.

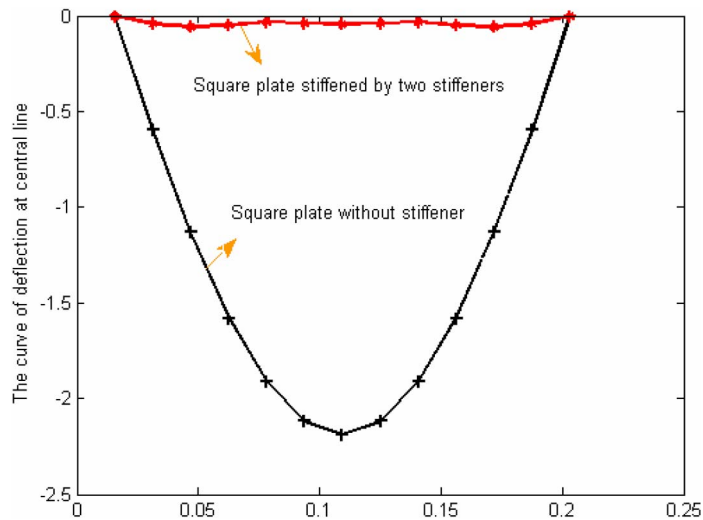


**Figure 9.** The decrease in deflection based on the number of stiffeners.

Next, a simply supported square plate stiffened by two stiffeners is studied as shown in Figure 8. The material properties and the value of the load are similar to those in the previous example. The influence of stiffeners on the deflection of plates is presented in Figure 9.

The last example in this section is a cylindrical shell roof that is supported on a rigid diaphragm on its curved boundaries. This structure with two eccentric stiffeners at the straight edges as shown in Figure 10 is studied. Geometric and material properties of the shell and the stiffener are given by  $R = 7.62$  m,  $t = 0.0762$  m,  $a = 15.24$  m,  $\alpha = 40^\circ$ ,  $h_s = 1.0$  m,  $b_s = 0.5$  m,  $E = 6.848 \times 10^{10}$  N/m<sup>2</sup>, and  $\nu = 0.3$ . We note that material properties of the shell and the stiffener are taken to be the same. This shell is subjected to an intensity of gravity load  $q = 4.393$  kN/m<sup>2</sup>; for the stiffener, the gravity load is considered as  $q_s = A_{\text{stiff}} \times \gamma_s$ , where  $\gamma_s = 24$  kN/m<sup>3</sup> and  $A_{\text{stiff}}$  is the cross-sectional area of the stiffener. Some available references related to this example are Omurtag and Akoz [28], Sinha [29], and Prusty and Satsangi [29]. In these references, this example was solved by using four-node rectangular elements for the shell and two-node bars for the stiffener in the model, triangular shallow shell elements based on a higher order strategy, and

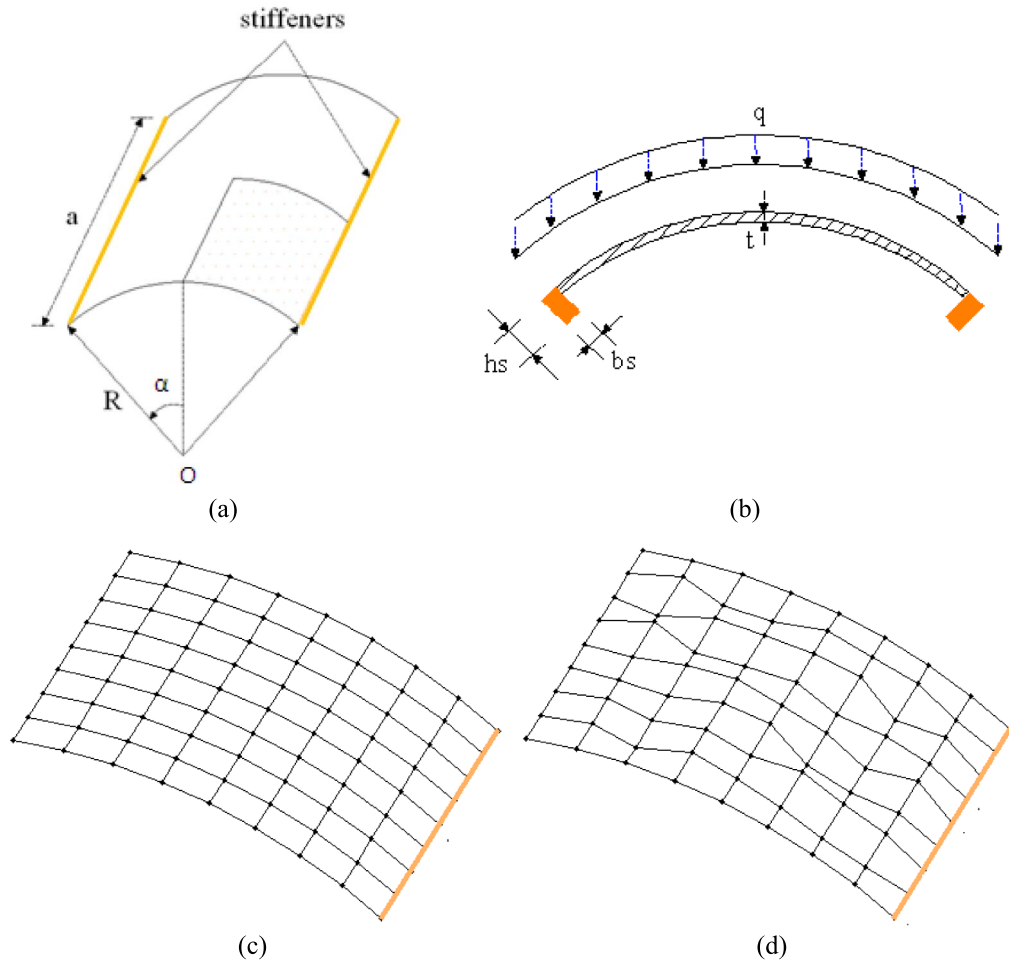


**Figure 10.** (a) The cylindrical shell roof stiffened by two stiffeners, (b) the cross-section, (c) regular mesh  $8 \times 8$  for a quarter, and (d) irregular mesh  $8 \times 8$  for a quarter with factor  $df=0.3$ .

eight-node isoparametric elements for the shell and three-node curved beam elements for the stiffener, respectively.

The convergence of central deflections of this shell roof with and without stiffeners by the SQ4C for the cases of regular ( $df = 0$ ) and irregular ( $df = 0.1, 0.2,$  and  $0.3$ ) meshes, together with the results by Omurtag and Akoz [28], Sinha [29], and Prusty and Satsangi [29], is presented in Table 2. Note that  $df$  is a controlling distortion factor. This factor is used to control the shapes of elements as given in [33].

### 6.2. Buckling analysis

One concentric stiffener is embedded in the simply supported square plate as shown in Figure 11. An in-plane load  $\sigma_x$  is applied on this structure. Three factors that are used for this structural analysis are given by  $\beta = L/B$ ,  $\gamma = EI_s/BD$ , and  $\delta = A_{stif}/BL$ , where  $I_s = b_s h_s^3/12$ ,  $D = Et^3/12(1 - \nu^2)$ , and  $A_{stif} = b_s h_s$ . The buckling parameter is defined by  $\lambda_{cr} = \lambda_{cr} L^2 / \pi^2 D$ .



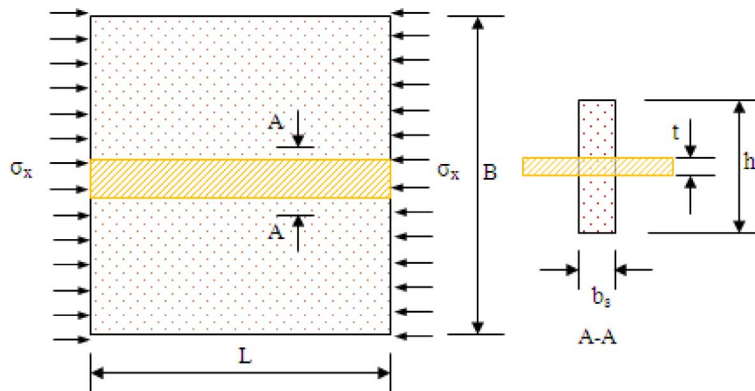


**Figure 11.** The square plate stiffened by one stiffener.

**Table 2.** Comparison of vertical deflection at the central point

| Deflection at central point (cm) | Unstiffened | Stiffened with $h_s = 1.0$ m and $b_s = 0.5$ m |
|----------------------------------|-------------|--|
| Omurtag and Akoz [28]            | 1.4200      | 0.1500   |
| Sinha [29]                       | 1.3300      | 0.1300   |
| Prusty and Satsangi [29]         | 1.4200      | 0.1759   |
| SQ4C (re)                        | 1.3517      | 0.1535   |
| SQ4C (irre, $df = 0.1$ )         | 1.3469      | 0.1501   |
| SQ4C (irre, $df = 0.2$ )         | 1.3414      | 0.1475   |
| SQ4C (irre, $df = 0.3$ )         | 1.3287      | 0.1390   |

**Table 3.** Comparison of the buckling parameter  $\bar{\lambda}_{cr}$

|                              |                          |                          |      |
|------------------------------|--------------------------|--------------------------|------|
| $\gamma = 5; \delta = 0.05$  | Timoshenko and Gere [51] | Trung <i>et al.</i> [22] | SQ4C |
| $\beta = 1$                  | 12.0                     | 11.7                     | 11.2 |
| $\beta = 2$                  | 8.2                      | 8.4                      | 8.7  |
| $\gamma = 10; \delta = 0.05$ | Timoshenko and Gere [51] | Trung <i>et al.</i> [22] | SQ4C |
| $\beta = 1$                  | 16.0                     | 16.2                     | 15.9 |
| $\beta = 2$                  | 10.3                     | 10.2                     | 11.4 |
| $\gamma = 15; \delta = 0.05$ | Timoshenko and Gere [51] | Trung <i>et al.</i> [22] | SQ4C |
| $\beta = 1$                  | 16.0                     | 16.3                     | 15.9 |
| $\beta = 2$                  | 12.5                     | 12.3                     | 13.6 |
| $\gamma = 20; \delta = 0.05$ | Timoshenko and Gere [51] | Trung <i>et al.</i> [22] | SQ4C |
| $\beta = 1$                  | 16.0                     | 16.2                     | 15.9 |
| $\beta = 2$                  | 14.7                     | 14.3                     | 14.5 |

The buckling parameters of this structure based on the change in the above factors are presented in Table 3. It can be seen that the solutions of this paper based on the SQ4C elements have a suitable convergence with the analytical solutions of Timoshenko and Gere [51] and the numerical solutions of Trung *et al.* [22]. Figure 12 plots the first six buckling mode shapes of

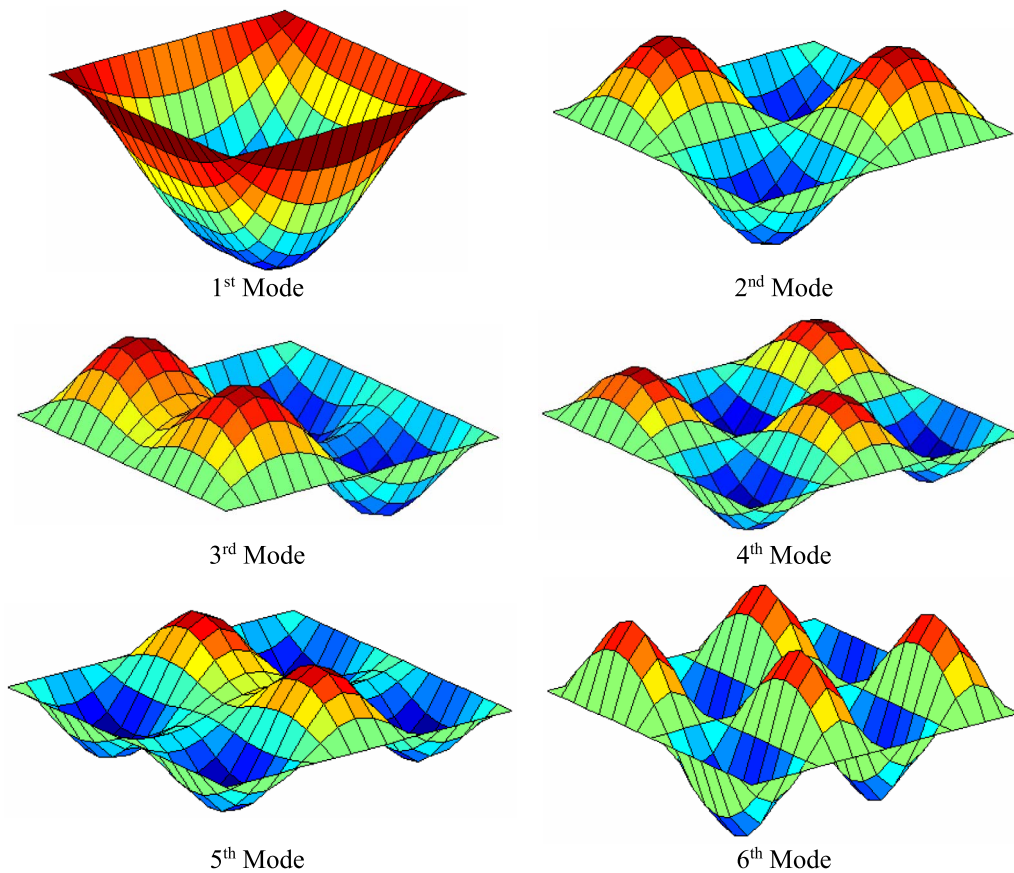


**Figure 12.** The first six buckling mode shapes with  $\beta = 1$ ,  $\gamma = 5$ , and  $\delta = 0.05$ .

the simple support square plate stiffened by one concentric stiffener and with  $\beta = 1$ ,  $\gamma = 5$ , and  $\delta = 0.05$ .

By changing the number of stiffeners, we study a simply supported square plate that is stiffened by  $n$  stiffeners as illustrated in Figure 13. Let  $n$  be equal to 1, 2, 3, 5, and 11. The parameters  $\gamma = 0.4$  and  $\delta = 0.02$  are used in this example.

The convergence of buckling parameters of this structure by the SQ4C, together with the results by Zhao [52], is presented in Figure 14.

Finally, an isotropic stiffened cylindrical shell is studied in this section as shown in Figure 15. The numbers of axial and circumferential stiffeners are 15 and 20. Let  $h_s = b_s = 1$  mm,  $E = 151$  GPa, and  $\nu = 0.3$ . The critical axial buckling loads for this structure with  $L/R = 1$  and  $R = 0.3$  m are listed in Table 4. It can be seen that the critical buckling loads by the SQ4C are in good agreement with the results by Almroth and Brush [53] and Farahani *et al.* [47].

## 7. Conclusions

The novel quadrilateral element, namely SQ4C, is presented and successfully applied to an analysis of stiffened plate/shell structures. Numerical analyses of statics and buckling have been conducted to verify the robustness of the proposed element. The present element can yield

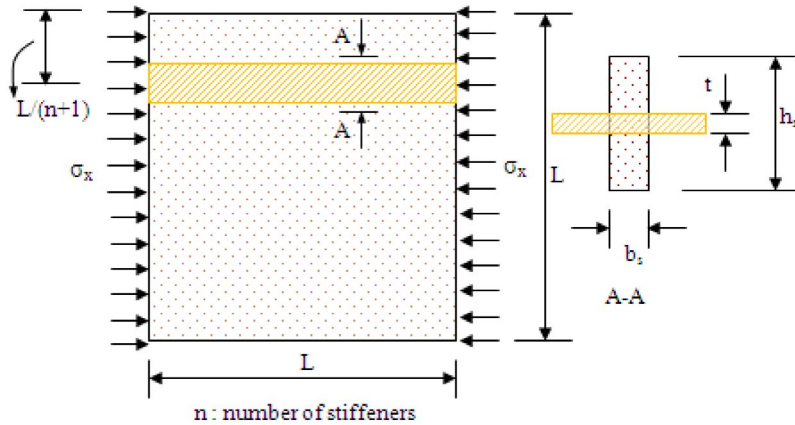


**Figure 13.** The square plate stiffened by  $n$  stiffeners.

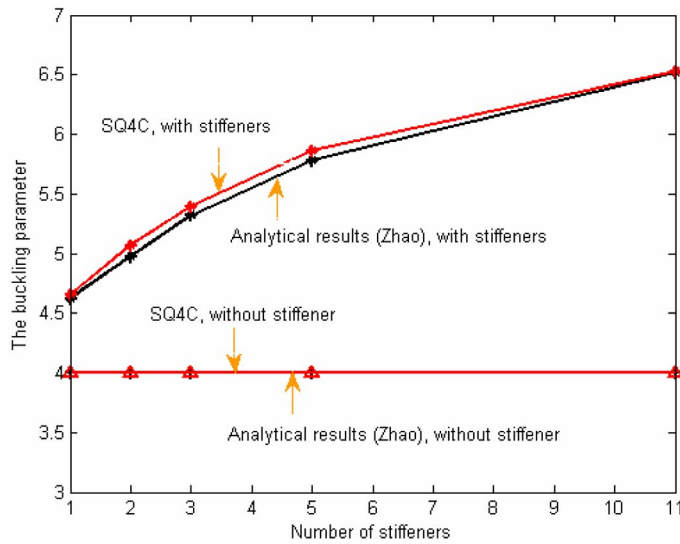


**Figure 14.** The buckling parameter of square plate stiffened by  $n$  stiffeners.

**Table 4.** Comparison of the critical axial buckling load (MN)

|               | Almroth and Brush [53] | Farahani <i>et al.</i> [47] | SQ4C (re) | SQ4C (irre, $df = 0.3$ ) |
|---------------|------------------------|-----------------------------|-----------|--------------------------|
| $t/R = 1/30$  | 26.3023                | 25.9558                     | 25.2167   | 25.2209                  |
| $t/R = 1/50$  | 9.4827                 | 9.4776                      | 9.5931    | 9.3937                   |
| $t/R = 1/100$ | 2.3659                 | 2.3743                      | 2.4840    | 2.4728                   |
| $t/R = 1/200$ | 0.5988                 | 0.5999                      | 0.5809    | 0.5823                   |
| $t/R = 1/300$ | 0.2672                 | 0.2686                      | 0.2604    | 0.2602                   |

satisfactory results in comparison with other available numerical results. In addition, the present element has the advantages of being simple in the formulation and implementation of static and buckling analyses of both plate and shell structures.

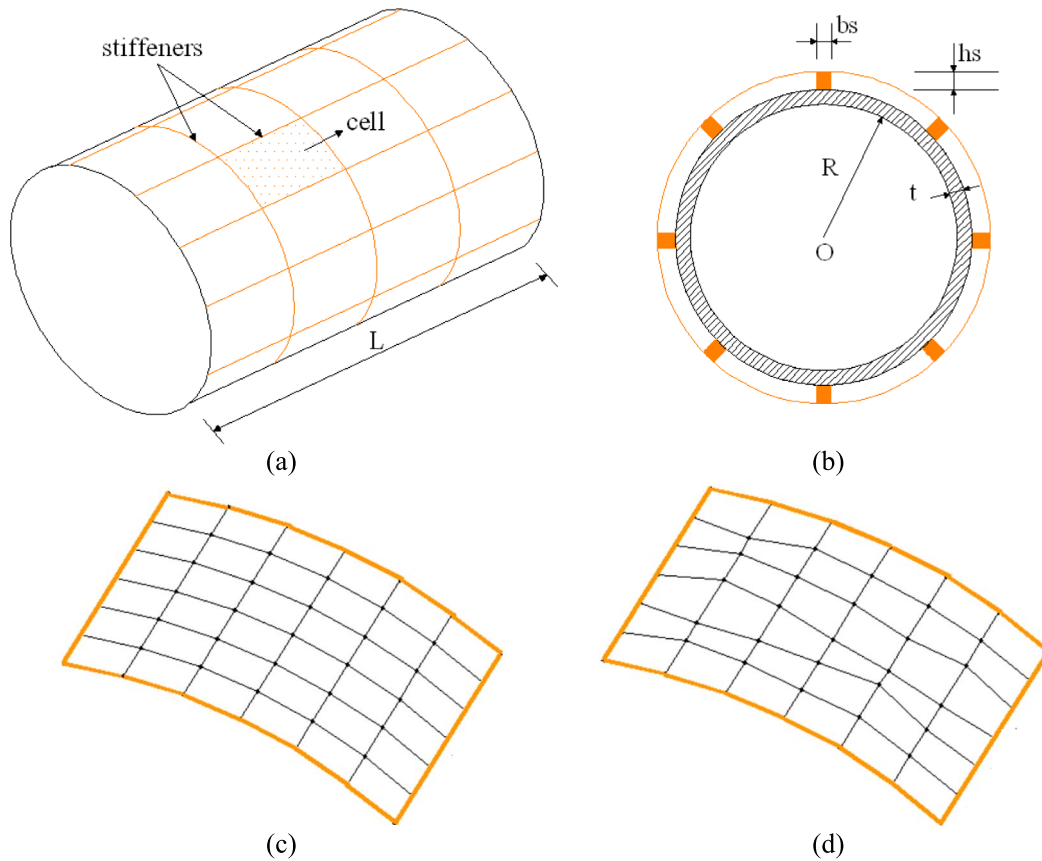


**Figure 15.** (a) The stiffened cylindrical shell, (b) the cross-section, (c) regular mesh  $6 \times 6$  for one cell, and (d) irregular mesh  $6 \times 6$  for one cell with factor  $df = 0.3$ .

## References

- [1] M. Mukhopadhyay, "Stiffened plates in bending", *Comput. Struct.* **50** (1994), p. 541-548.
- [2] Y. Pan, L. A. Louca, "Experimental and numerical studies on the response of stiffened plates subjected to gas explosions", *J. Constr. Steel Res.* **52** (1999), p. 171-193.
- [3] A. Samanta, M. Mukhopadhyay, "Finite element large deflection static analysis of shallow and deep stiffened shells", *Finite Elem. Anal. Des.* **33** (1999), p. 187-208.
- [4] A. E. Assan, "Analysis of multiple stiffened barrel shell structures by strain-based finite elements", *Thin-Walled Struct.* **35** (1999), p. 233-253.
- [5] A. Rittweger, T. Schermann, H. G. Reimerdes, H. Öry, "Influence of geometric imperfections on the load capacity of orthotropic stiffened and composite shells of revolution with arbitrary meridians and boundary conditions", *Thin-Walled Struct.* **23** (1995), p. 237-254.
- [6] R. Brian, "Nonlinear rigid-plastic analysis of stiffened plates under blast loads", PhD thesis, University of British Columbia, 1991.
- [7] C. Bisagni, R. Vescovini, "Analytical formulation for local buckling and post-buckling analysis of stiffened laminated panels", *Thin-Walled Struct.* **47** (2009), p. 318-334.
- [8] B. H. S. Oliveira, E. L. Neto, F. A. C. Monteiro, "An accurate Ritz approach for analysis of cracked stiffened plates", *Appl. Math. Modelling* **73** (2019), p. 598-614.
- [9] V. Gulizzi, V. Oliveri, A. Milazzo, "Buckling and post-buckling analysis of cracked stiffened panels via an X-Ritz method", *Aerosp. Sci. Technol.* **86** (2019), p. 268-282.
- [10] V. Oliveri, A. Milazzo, "A Rayleigh-Ritz approach for postbuckling analysis of variable angle tow composite stiffened panels", *Comput. Struct.* **196** (2018), p. 263-276.

- [11] O. D. de Matos Junior, M. V. Donadon, S. G. P. Castro, "Aeroelastic behavior of stiffened composite laminated panel with embedded SMA wire using the hierarchical Rayleigh–Ritz method", *Compos. Struct.* **181** (2017), p. 26-45.
- [12] L. X. Peng, K. M. Liew, S. Kitipornchai, "Buckling and free vibration analyses of stiffened plates using the FSDT mesh-free method", *J. Sound Vib.* **289** (2006), p. 421-449.
- [13] L. X. Peng, K. M. Liew, S. Kitipornchai, "Analysis of stiffened corrugated plates based on the FSDT via the mesh-free method", *Int. J. Mech. Sci.* **49** (2007), p. 364-378.
- [14] K. M. Liew, S. Kitipornchai, L. X. Peng, "4 - Mesh-free methods for buckling analysis of stiffened and corrugated plates", in *Analysis and Design of Plated Structures* (N. E. Shanmugam, C. M. Wang, eds.), vol. 2, Woodhead Publishing, 2006, p. 80-116.
- [15] M. P. Rossow, A. K. Ibrahimkhail, "Constraint method analysis of stiffened plates", *Comput. Struct.* **8** (1978), p. 51-60.
- [16] J. N. Kamineni, R. G. Burela, "Constraint method for laminated composite flat stiffened panel analysis using variational asymptotic method (VAM)", *Thin-Walled Struct.* **145** (2019), article ID 106374.
- [17] X. Q. Zhou, D. Y. Yu, X. Shao, S. Wang, Y. H. Tian, "Band gap characteristics of periodically stiffened-thin-plate based on center-finite-difference-method", *Thin-Walled Struct.* **82** (2014), p. 115-123.
- [18] M. Mukhopadhyay, "Vibration and stability analysis of stiffened plates by semi-analytic finite difference method. Part I: Consideration of bending displacements only", *J. Sound Vib.* **130** (1989), p. 27-39.
- [19] A. S. Rajawat, A. K. Sharma, P. Gehlot, "Free vibration analysis of stiffened laminated plate using FEM", *Materials Today: Proceedings* **5** (2018), p. 5313-5321.
- [20] P. Gehlot, A. K. Sharma, A. S. Rajawat, "Harmonic analysis of stiffened functionally graded plate using FEM", *Materials Today: Proceedings* **5** (2018), p. 5145-5153.
- [21] L. Li, R. Xiaohui, "Stiffened plate bending analysis in terms of refined triangular laminated plate element", *Compos. Struct.* **92** (2010), p. 2936-2945.
- [22] T. Nguyen-Thoi, T. Bui-Xuan, P. Phung-Van, H. Nguyen-Xuan, P. Ngo-Thanh, "Static, free vibration and buckling analyses of stiffened plates by CS-FEM-DSG3 using triangular elements", *Comput. Struct.* **125** (2013), p. 100-113.
- [23] R. K. Behera, S. S. Patro, N. Sharma, K. K. Joshi, "Eigen-frequency analysis of stiffened laminated composite plates using finite elements", *Mater. Today: Proceedings* **5** (2018), p. 20152-20159.
- [24] M. S. Bouabdallah, J. L. Batoz, "Formulation and evaluation of a finite element model for the linear analysis of stiffened composite cylindrical panels", *Finite Elem. Anal. Des.* **21** (1996), p. 265-289.
- [25] Z. Zhang, H. Chen, L. Ye, "Progressive failure analysis for advanced grid stiffened composite plates/shells", *Compos. Struct.* **86** (2008), p. 45-54.
- [26] Z. Ni, K. Zhou, X. Huang, H. Hua, "Free vibration of stiffened laminated shells of revolution with a free-form meridian and general boundary conditions", *Int. J. Mech. Sci.* **157–158** (2019), p. 561-573.
- [27] G. G. Sheng, X. Wang, "The dynamic stability and nonlinear vibration analysis of stiffened functionally graded cylindrical shells", *Appl. Math. Modelling* **56** (2018), p. 389-403.
- [28] M. Omurtag, A. Y. Aköz, "Mixed finite element formulation of eccentrically stiffened cylindrical shells", **42** (1992).
- [29] B. G. Prusty, S. K. Satsangi, "Analysis of stiffened shell for ships and ocean structures by finite element method", *Ocean Eng.* **28** (2001), p. 621-638.
- [30] I. Katili, J.-L. Batoz, I. J. Maknun, A. Hamdouni, O. Millet, "The development of DKMQ plate bending element for thick to thin shell analysis based on the Naghdi/Reissner/Mindlin shell theory", *Finite Elem. Anal. Des.* **100** (2015), p. 12-27.
- [31] L. Leonetti, H. Nguyen-Xuan, "A mixed edge-based smoothed solid-shell finite element method (MES-FEM) for laminated shell structures", *Compos. Struct.* **208** (2019), p. 168-179.
- [32] B. Liu, S. Lu, J. Ji, A. J. M. Ferreira, C. Liu, Y. Xing, "Three-dimensional thermo-mechanical solutions of cross-ply laminated plates and shells by a differential quadrature hierarchical finite element method", *Compos. Struct.* **208** (2019), p. 711-724.
- [33] H. Nguyen-Van, N. Nguyen-Hoai, T. Chau-Dinh, T. Nguyen-Thoi, "Geometrically nonlinear analysis of composite plates and shells via a quadrilateral element with good coarse-mesh accuracy", *Compos. Struct.* **112** (2014), p. 327-338.
- [34] T. Q. Bui, T. V. Do, L. H. T. Ton, D. H. Doan, S. Tanaka, D. T. Pham *et al.*, "On the high temperature mechanical behaviors analysis of heated functionally graded plates using FEM and a new third-order shear deformation plate theory", *Compos. Part B: Eng.* **92** (2016), p. 218-241.
- [35] L. T. That-Hoang, H. Nguyen-Van, T. Chau-Dinh, C. Huynh-Van, "Enhancement to four-node quadrilateral plate elements by using cell-based smoothed strains and higher-order shear deformation theory for nonlinear analysis of composite structures", *J. Sandwich Struct. Mater.* **22** (2018), no. 7, p. 2302-2329.
- [36] H. L. Ton-That, H. Nguyen-Van, T. Chau-Dinh, "An improved four-node element for analysis of composite plate/shell structures based on twice interpolation strategy", *Int. J. Comput. Methods* **17** (2020), no. 6, article ID 1950020.
- [37] H. Nguyen-Van, H. L. Ton-That, T. Chau-Dinh, N. D. Dao, "Nonlinear Static Bending Analysis of Functionally Graded

- Plates Using MISQ24 Elements with Drilling Rotations”, in *Proceedings of the International Conference on Advances in Computational Mechanics 2017*, Springer Singapore, 2018, p. 461-475.
- [38] N. Nguyen-Thanh, K. Zhou, X. Zhuang, P. Areias, H. Nguyen-Xuan, Y. Bazilevs *et al.*, “Isogeometric analysis of large-deformation thin shells using RHT-splines for multiple-patch coupling”, *Comput. Methods Appl. Mech. Eng.* **316** (2017), p. 1157-1178.
- [39] J. h. Lim, D. Sohn, S. Im, “Variable-node element families for mesh connection and adaptive mesh computation”, *Struct. Eng. Mech.* **43** (2012), p. 349-370.
- [40] H. L. T. That, H. Nguyen-Van, T. Chau-Dinh, “Nonlinear bending analysis of functionally graded plates using SQ4T elements based on twice interpolation strategy”, *J. Appl. Comput. Mech.* **6** (2019), no. 1, p. 125-136.
- [41] K.-J. Bathe, E. N. Dvorkin, “A formulation of general shell elements—the use of mixed interpolation of tensorial components”, *Int. J. Numer. Methods Eng.* **22** (1986), p. 697-722.
- [42] K.-J. Bathe, E. N. Dvorkin, “A four-node plate bending element based on Mindlin/Reissner plate theory and a mixed interpolation”, *Int. J. Numer. Methods Eng.* **21** (1985), p. 367-383.
- [43] E. N. Dvorkin, S. I. Vassolo, “A quadrilateral 2-D finite element based on mixed interpolation of tensorial components”, *Eng. Comput.* **6** (1989), p. 217-224.
- [44] Y. Ko, P.-S. Lee, K.-J. Bathe, “The MITC4+ shell element and its performance”, *Comput. Struct.* **169** (2016), p. 57-68.
- [45] Y. Ko, P.-S. Lee, K.-J. Bathe, “The MITC4+ shell element in geometric nonlinear analysis”, *Comput. Struct.* **185** (2017), p. 1-14.
- [46] Y. Ko, P.-S. Lee, K.-J. Bathe, “A new MITC4+ shell element”, *Comput. Struct.* **182** (2017), p. 404-418.
- [47] H. Farahani, R. Azarafza, F. Barati, “Mechanical buckling of a functionally graded cylindrical shell with axial and circumferential stiffeners using the third-order shear deformation theory”, *C. R. Méc.* **342** (2014), p. 501-512.
- [48] C. Chang-Koon, L. Tae-Yeol, “High performance variable-node element libraries for structural engineering applications”, in *Computational Mechanics—New Frontiers for the New Millennium* (S. Valliappan, N. Khalili, eds.), Elsevier, Oxford, 2001, p. 187-194.
- [49] L. Ton That, “Finite element analysis of functionally graded skew plates in thermal environment based on the new third-order shear deformation theory”, *J. Appl. Comput. Mech.* **6** (2019), no. 4, p. 1044-1057.
- [50] A. Ibrahimbegovic, R. L. Taylor, E. L. Wilson, “A robust quadrilateral membrane finite element with drilling degrees of freedom”, *Int. J. Numer. Methods Eng.* **30** (1990), p. 445-457.
- [51] S. Timoshenko, J. Gere, *Theory of Elastic Stability*, 2nd ed., McGraw-Hill Book Company, Inc., Toronto, 1961, New York.
- [52] W. Zhao, “Buckling analysis of stiffened plates with straight and curvilinear stiffener(s)”, Virginia Tech2013.
- [53] D. O. Brush, B. O. Almroth, *Buckling of Bars, Plates and Shells*, McGraw-Hill, New York, 1975.